UNIVERSITY of CALIFORNIA
SANTA CRUZ

OPERATION OF THE PROSPECTIVE SID BEAMCAL IN THE EXPECTED HIGH-RADIATION FORWARD ENVIRONMENT OF THE ILC

A thesis submitted in partial satisfaction of the
requirements for the degree of

BACHELOR OF SCIENCE

in

PHYSICS

by

Benjamin Randolph Smithers

April 13 2018

The thesis of Benjamin Randolph Smithers is approved by:

Professor Bruce Schumm
Advisor

Professor David P. Belanger
Theses Coordinator

Professor Robert P. Johnson
Chair, Department of Physics

Abstract

Operation of the Prospective SiD BeamCal in the Expected High-Radiation Forward Environment of the ILC

by

Benjamin Randolph Smithers

FLUKA Monté Carlo simulations were used to simulate the environmental conditions the International Linear Collider's Silicon Detector's BeamCal will sustain during operation. By using a GunieaPig simulated bunch crossing for primary particles, and the T-506 experimental results, I estimate that after one Snowmass year of usage the BeamCal will draw on the order of 10^2 Watts while operating at -10°C and at a bias voltage of 600V. This wattage will be significantly lower if operated at cooler temperatures. The sensitive electronics mounted radially around the BeamCal will endure minimal BeamCal-sourced non-neutron radiation.

Contents

List of Figures

List of Tables

Acknowledgements

I would like to thank my parents, brother, and nearby aunt and uncle for their support of me throughout my youth and collegiate career, and their encouragement in my pursuing a higher education. I would also like to thank my thesis advisor Bruce Schumm for fostering my interest in high energy physics, and motivating the FLUKA project below.

1

Introduction

1.1 The International Linear Collider

The International Linear Collider, or ILC, is a proposed electron-positron collider scheduled to begin construction in the 2020s in the mountainous northern regions of Japan. In its baseline design, the 30km long linear collider will operate with a center of mass energy of 500 GeV and be capable of focusing the beams to extreme precision and achieving a luminosity of $2 \times 10^{34}\text{cm}^2\text{s}^{-1}$. Although the collisions are to be lower in energy than CERN's discovery-focused Large Hadron Collider, the ILC will be capable of high-precision measurements and is designed to accurately measure the Higgs particle's spin and test aspects of supersymmetry, should it be found in nature.

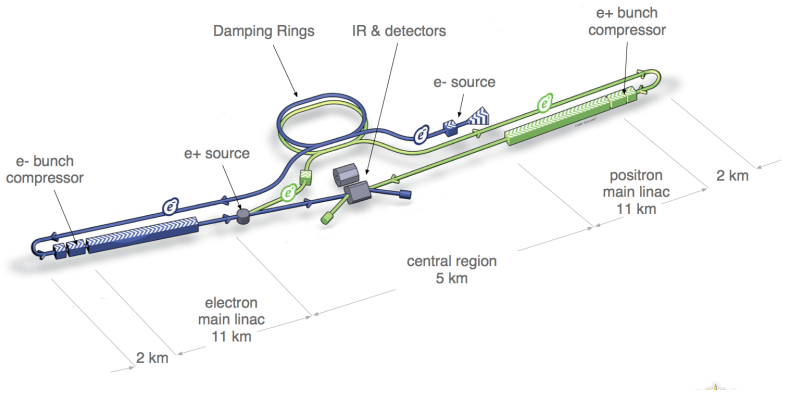

Figure 1.1: The arrangement of ILC components, sourced from "https://www.linearcollider.org/images/"

A requirement of the ILC's design is the longevity and continued functionality of its subcomponents. The T-506 experiment at the SLAC End Station A Test Beam facility [2] studied the effects of electromagnetically induced radiation on prospective sensors that might be used for far forward calorimetry at the ILC - the one region of the detector for which radiation rates will be significant. The T-506 results provide the experimental basis from which it is possible to produce damage estimates to and around the ILC's far-forward Beamline Calorimeter (BeamCal) over the course of such a device's operation. Here, I present a study using the FLUKA simulation framework [3][4] that extrapolates the T-506 results to develop expectations for BeamCal performance as it accumulates its expected radiation dose.

1.2 The BeamCal

The BeamCal is a detector to be placed far forward of the particle interaction point, as shown in Fig. 1.2, and is composed of fifty alternating layers of tungsten radiators and solid-state sensors. Its function is to reconstruct beam parameters by detecting electrons

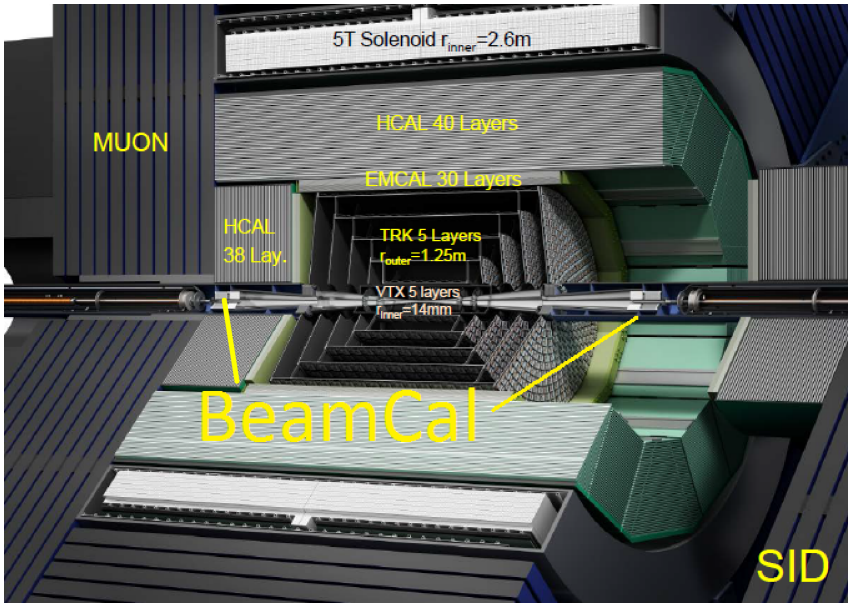

Figure 1.2: Location of BeamCal in SiD. Image modified, sourced from "The SiD Detector at ILC" by Tim Barklow, "https://indico.cern.ch/"

and positrons pair-produced by the fusion of *Beam*strahlung[1] photons, which are drawn from a virtual photon cloud surrounding the beams' bunches of particles as they collide. There are 2×10^{10} particles in a bunch, 1312 bunches in 0.73ms *trains*, and 5 trains crossing the interaction region every second.

The electron-positron pairs tend to be only slightly divergent from the beam path, and this irradiates the most forward element of the ILC detector with particle energies in the 10s of MeV to GeV range. This high-energy radiation, which amounts to a total of about 10 TeV per bunch crossing, could pose a threat to the longevity of the BeamCal itself as well as the electronics around it. Through this study I hope to understand the effects of the pair background and to provide benchmarks for the engineering requirements of the electronics around the BeamCal and the solid-state sensors within it.

The potentially damaging radiation arises from the showers of electromagnetic particles (e+, e-, γ) resulting from the particle flux of e+e- pairs onto the BeamCal. These

[1]Brehms- is the radiation from charged particles interacting with and passing through matter, Beams- is the radiation from a beam interacting with the fields of another beam.

pairs induce electromagnetic showers, the constituent photons of which excite the Giant Dipole Resonance of nuclei in the BeamCal's tungsten plates, which then decay through neutron evaporation. The resulting neutron bombardment can damage the Silicon sensors in the BeamCal and other electronics around the BeamCal. One way this damage manifests is a dark current (leakage current) that flows when the sensors are energized. This contributes to extra power consumption in the BeamCal sensors that must be drawn out in order to avoid damage; increasing the complexity of the BeamCal design and the expense of its construction and operation. Sensors must be chosen such that these effects are minimized, and it is the purpose of this study to investigate the use of silicon sensors in the BeamCal.

2

Numerical Simulation

To proceed it was necessary to understand characteristics of the neutron field and the electromagnetic showers formed within and around the BeamCal while it is subject to the expected electron-positron pair background. Due to the system's complexity numerical simulations are necessary. Since the simulations must support photonuclear interactions and neutron transport, I used the Monté Carlo framework FLUKA[1] for simulating the development of the electromagnetic shower and its hadronic (neutron) component in the BeamCal. The FLUKA simulation made uses a list of electron-positron pairs, along with their energies and trajectories, produced via the GuineaPig Beam-Beam simulation program[5].

Installation of FLUKA and FLUKA-related utilities (FLUKA Flair and Flair Geoviewer [6]) requires the latest versions of the gfortran compiler, Gnuplot, a python interpreter, Tcl/Tk, and the Tkinter toolkit. Several developer releases are also required: python-imaging, python-imaging-tk, tk-dev, and python-dev. I installed FLUKA on a dedicated server, pulled from a pool of unused equipment at SCIPP, that I had procured for this purpose. The server was set up in a faculty office at the SCIPP institute.

[1]The name is derived from *FLUktuierende KAskade*, German for *fluctuating cascade*

2.1 Using FLUKA

Once operational, FLUKA accepts an ASCII formatted text file, called the "input file," to define basic simulations parameters. Each row within the input file is called a "card," and it is through a series of these cards that a FLUKA user establishes the simulation geometry, primary particle or beam properties, scoring (detection) methods, and other basic settings. There are two ways of preparing these input files: typing the input file by hand or using the FLUKA Flair graphical user interface.

Although input file cards alone can be used for most simulation needs, niche uses often require specially written "user routines." User routines are written in Fortran and compiled using the FLUKA `fff` Fortran compiler script. The script is intended for tcsh users, and so BASH users must modify the first line in the `fff` script to read `#!/bin/bash`. After successfully compiling the user-routine into a Fortran executable, one then links the compiled executable and any other desired `fff` compiled executables to the FLUKA executable by use of the FLUKA `lfluka` script. No modifications to `lfluka` are required for BASH users. User routines I created for this study include `beamcalSource`, used to load the electron-positron pair background into the primary particle list used for FLUKA simulations; and `beamcalDraw` for outputting detailed information regarding the neutron energies and trajectories for use as collision tape in later experiments.

2.2 Output from FLUKA

FLUKA has a variety of options regarding the output for simulations, which are chosen following the `SCORE` card in the input file or defined specifically using a user routine. The scoring process keeps track of the particles penetrating a specified surface

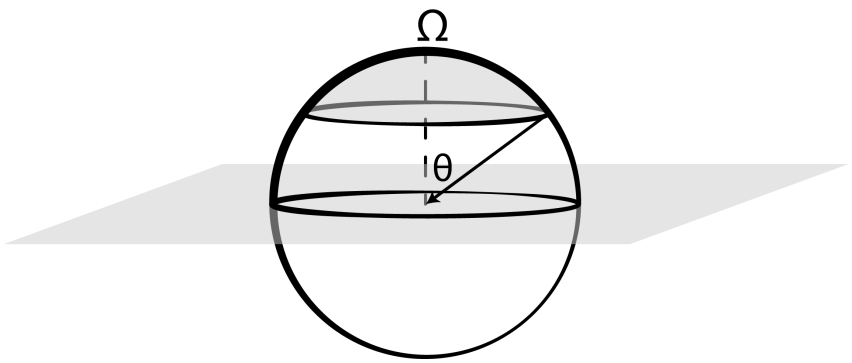

Figure 2.1: Illustration of relation between trajectory angle θ and solid angle Ω.

in space. Typically, a user specifies the Fortran unit number used for scoring data before it is output to a file, whether the final output should be formatted or unformatted[2], the binning methods used in scoring, what particles to score, and where to place the scoring surface. Most often this will be a particle fluence through a surface binned and scaled per GeV and/or steradian. FLUKA angular variables are defined as the angle between particle trajectory and the scoring surface's normal vector. Using this assumption, FLUKA correlates solid angle Ω with θ by integrating over part of a unit-sphere's surface:

$$\Omega = \int_{\phi=0}^{\phi=2\pi} \int_{\theta'=0}^{\theta'=\theta} \sin\theta' d\theta' d\phi,$$

illustrated in Fig. 2.1. This yields the relation

$$1 - \frac{\Omega}{2\pi} = \cos\theta. \tag{2.1}$$

Equation (2.1) is necessary when correlating "angular bins" in FLUKA with bins of particle angle of incidence.

I recommend that future FLUKA users choose to output data from simulations as unformatted, and then reformat the data using the appropriate fluka script. This will

[2]a text file or binary file

yield a machine-readable tab-delineated data file, while FLUKA's methods of outputting simulation data directly to a formatted file yields a structure difficult to make machine-readable[3].

To elaborate, if one uses the `SCORE` type card `USRBDX` to score with respect to energy and solid-angle, they may then specify to output unformatted. Later, they would pass the output data file through `USRBDX`'s associated script `usxsuw`; this produces a sectioned text file. Each section corresponds to a range in Ω, and has an array of data values four columns wide with a row for each requested energy bin: the first and second entries in a row are edges of the energy bin, the third entry is the quantity scored in this energy and Ω range, and the fourth entry is the statistical uncertainty of that measurement. The quantity scored, such as fluence Φ (defined below), is normalized by the widths of that bin and the number of primary particles in the simulation; yielding a discretized double differential distribution $\left(\frac{d^2\Phi}{dEd\Omega}\right)$.

2.3 Fluence

As most of my simulations involve the fluence of neutrons, it is important that I distinguish the characteristics of *fluence* with those of the more common term *flux*. Put simply, flux is the passage of 'stuff' per unit area per unit time, or particles/cm^2/sec through a surface.

Fluence, on the other hand, is defined by the International Commission on Radiation Units and Measurements as a time-integrated total pathlength of particles passing through a volume:

$$\Phi = \frac{dl}{dV}, \tag{2.2}$$

[3]for those curious, FLUKA prints numbers out like words in a paragraph

in cm^{-2}, where dl is the sum of all pathlengths through the volume dV [7]. Note: this is not a derivative, but a ratio of small values. To compare these two quantities, suppose n particles pass through a surface of area A and depth d at angles of incidence θ_i over t seconds. The flux and fluence of particles are respectively

$$\text{Flux:} \qquad \text{Fluence:} \tag{2.3}$$

$$\phi = \frac{n}{At} \qquad \Phi = (dl)\,\frac{1}{dV} = \left(\sum_{i=1}^{n} \frac{d}{\cos\theta_i}\right)\frac{1}{Ad} = \sum_{i=1}^{n} \frac{1}{A\cos\theta_i}, \tag{2.4}$$

where again, dl is the sum of all path lengths. As the thickness d falls out of the fluence expression, fluence can therefore be calculated for any infinitesimally thin surface. In fact, fluences in FLUKA are measured across two-dimensional boundaries. A fluence of neutrons has units (neutrons-cm^{-2}).

2.4 Specific FLUKA Settings

I called a variety of specific cards to allow for the efficient and accurate performance of all FLUKA simulations described later. These cards and their effects are described as follows:

- the DEFAULTS card with SDUM = "PRECISIO". This allows low energy neutron transport down to thermal energies along with several other options for precision simulations. The online FLUKA manual describes this option in detail.

- the PHYSICS card with SDUM = "EVAPORAT" to enable FLUKA's models for nuclear evaporation. I used the new evaporation model with no heavy fragment evaporation.

- the PHOTONUC card for enabling FLUKA's model of photonuclear interactions. Arguments were set such that giant dipole resonance interactions, quasi-deuteron interactions, high-energy (>0.7GeV) interactions, and interactions in the region of the delta resonance are all allowed.

- the LAM-BIAS card to bias photonuclear interactions in Tungsten; reducing the hadronic inelastic interaction length of electrons, positrons, neutrinos, anti-neutrinos, and photons by a factor of 0.09. This allows certain interactions to happen more frequently, but treats the daughter particles as fractions of particles.

I used the `USRBDX` card to score neutrons through patches of varying sizes, and output the fluence through this patch into an unformatted data file with 60 angular bins and 300 energy bins, which I reformatted using `USRBDX`'s `usxsuw` script. Analysis of these formatted data files would be done using various python scripts.

3

Applying Simulation Results

3.1 SLAC End Station A Test Beam Experiment T-506

Understanding the effects on the BeamCal requires a quantifiable metric for measuring damage to Silicon crystal particle sensors. For this purpose, we assume the following:

1. The Non-Ionizing Energy Loss (NIEL) Scaling Hypothesis - as described below.

2. Leakage current scales exponentially with temperature.

3. As follows from the NIEL Scaling Hypothesis, leakage current scales linearly with dosage.

These assumptions are supported by numerous observations. First, NIEL scaling hypothesis has been shown to be valid under most circumstances, including the cases of neutron-induced radiation on silicon sensors. Meanwhile, the behavior of leakage current with respect to temperature follows from Maxwell-Boltzman statistics, which describe

Surface	Location [cm]
R1 Entrance	0.0
R1 Exit	0.7
R2 Entrance	46.6
R2 Exit	48.0
Sensor	48.5
R3 Entrance	49.4
R3 Exit	52.2

Table 3.1: Location of the various tungsten radiator elements and the sensor under irradiation for the T-506 experiment. The R1 radiator had thickness $2X_0^W$, and the R2 and R3 radiators had thicknesses $4X_0^W$ and $8X_0^W$ respectively.

how occupation in the conduction band of solid state materials scales exponentially with respect to temperature.

The T-506 experiment run at the SLAC End Station A Test Beam (ESTB) facility serves as an experimental baseline from which the FLUKA simulations can be used to extrapolate to other detector systems. In the T-506 experiment, researchers placed various types of solid-state sensors in the midst of a tungsten radiator, and subjected these detectors to various dosages using the End Station A electron beam scanned over a 1cm^2 area. They then measured the detectors' leakage currents and charge collection efficiency at varying bias voltages and temperatures at varying stages of annealing(heat treatment)[2].

The apparatus itself consisted of three tungsten plates, each with a thickness a multiple of Tungsten's radiation length X_0^W. The dimensions are given in Table 3.1 [2], and the geometric layout was designed in order to recreate the balance of particles likely to be found in an operational BeamCal. The T-506 study made use of here was a 51 μC exposure of a p-bulk silicon diode sensor. The 13.3 GeV electron beam was directed over the sensor over a period of approximately one day. This exposure corresponds to a cumulative ionizing dose of 270 Mrad. The sensor's leakage current and charge collection

Temperature [°C]	Current [A]	Normalized Current [A cm^{-2}]
21.8	52.0×10^{-6}	2.08×10^{-3}
13.9	25.7×10^{-6}	1.03×10^{-3}
6.95	14.7×10^{-6}	5.90×10^{-4}
0.0	5.23×10^{-6}	2.09×10^{-4}
-7.43 C	2.09×10^{-6}	8.35×10^{-5}
-14.87	1.15×10^{-6}	4.60×10^{-5}

Table 3.2: Leakage current of T-506 WSI-P4 p-bulk silicon diode sensor, irradiated to 270 Mrad, with respect to temperature at a 600V bias.

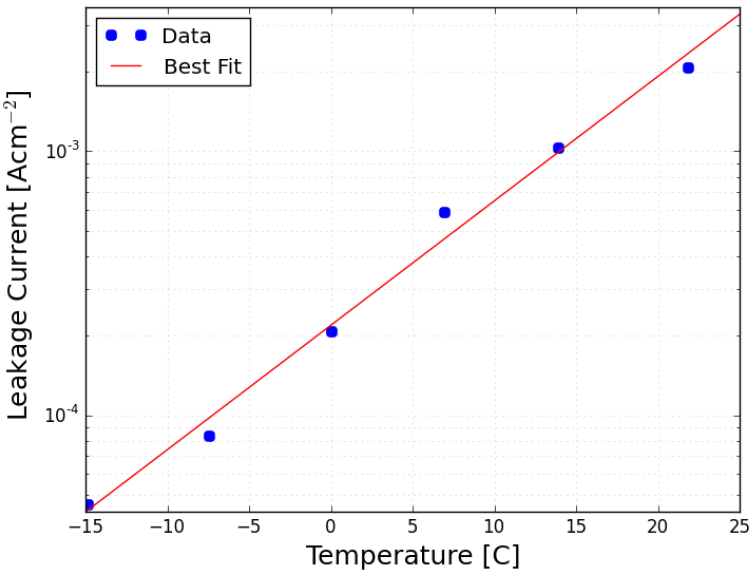

Figure 3.1: T-506 leakage current vs temperature, data with best fit of $\sigma(T) \equiv (2.19 \times 10^{-4}) \exp(0.11T)$.

efficiency were evaluated after a series of one-hour annealing steps at increasing temperatures. While annealing had little effect on leakage current, it was observed to lower the sensor's depletion voltage for temperatures up to 80°C. At a bias voltage of 600V, close to full depletion, the charge collection efficiency was observed to be 80% of sensor's original value. These leakage current data at various temperatures are presented in Table 3.2[2], and a fit with the data are plotted in Fig. 3.1. By the fit, a leakage current of 74.1 μA-cm^{-2} would be measured at -10.0°C and the same bias voltage.

I then recreated the T-506 apparatus in FLUKA according to the experimental pa-

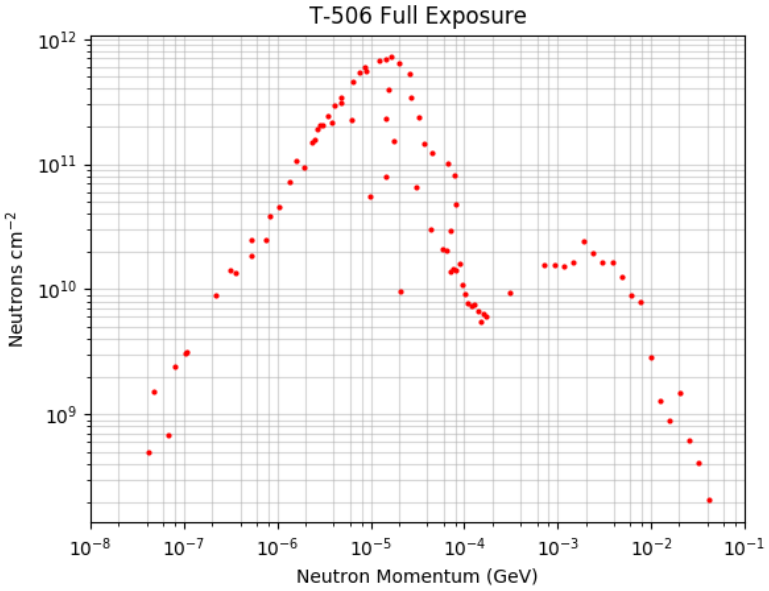

Figure 3.2: Number of neutrons scored during FLUKA simulation of the T-506 apparatus per unit area per primary beam particle. Plot generated with matplotlib and using output datafile from FLUKA simulation.

rameters, and ran the simulation over 5×10^5 primaries, and analyzed the output file using a custom-made python script. The total count rates of neutrons with respect to energy is show in Fig. 3.2.

A common unit associated with neutron-induced damage is Φ_{eq}, the equivalent fluence of 1MeV Neutrons. To calculate it, we consider Assumption (1), the **Non-Ionizing Energy Loss (NIEL) Scaling Hypothesis**. The NIEL Hypothesis posits that damage affects due to energetic particles in the bulk of a material are proportional to the NIEL experienced by those particles [8] (See Fig. 3.3 for NIEL vs energy for through-going neutrons in silicon). For a fluence of neutrons of varying energies, the equivalent fluence of 1MeV neutrons is calculated by scaling each component neutron's fluence by the ratio of its NIEL and the 1MeV NIEL and summing over all scaled fluence. That is,

$$\Phi_{eq} = \sum_E \Phi(E) \frac{\text{NIEL}(E)}{\text{NIEL(1MEV)}}. \tag{3.1}$$

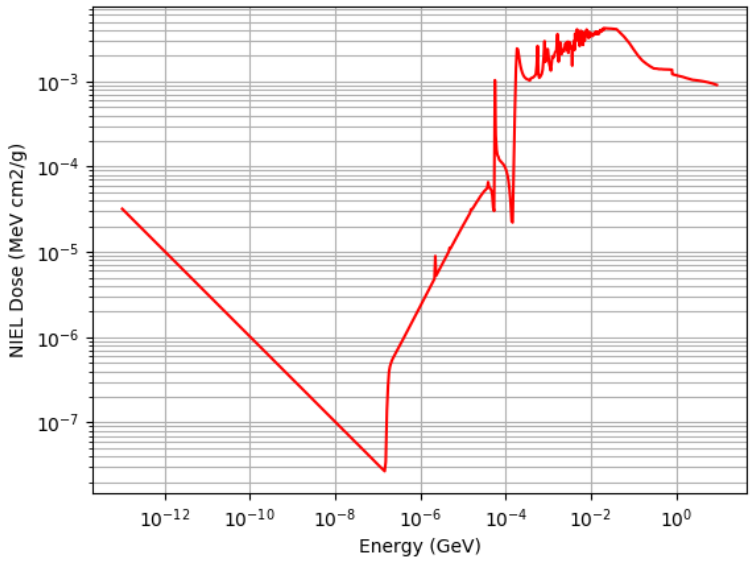

Figure 3.3: Non-Ionizing Energy Loss function NIEL(E) of Neutrons in Silicon[8].

When modified to reflect the output from FLUKA simulations Eq. (3.1) becomes

$$\Phi_{eq} = \sum_{\text{bins}} \frac{\Phi(E,\theta)}{dEd\Omega} \frac{\text{NIEL}(E)}{\text{NIEL}(1\text{MeV})} dEd\Omega. \tag{3.2}$$

By integrating over the bins of the T-506 FLUKA simulation output using a python script and above measure, the T-506 experiment corresponds to an equivalent fluence Φ_{eq} of 0.19 1MeV Neutrons cm^{-2} per 13.3 GeV primary electron at the location of the sensor. As 51 μC were delivered to the apparatus, the beam consisted of 3.25×10^{14} beam electrons. The total equivalent fluence of 1MeV neutrons was therefore 6.17×10^{13} cm^{-2}.

3.2 Comparison to Previous Results

The RD48 collaboration, G Lindström et al, subjected a variety of sensors to a neutron source to study the effects of neutron-induced damage, and found that leakage current

depended only on the equivalent fluence of 1MeV neutrons (Φ_{eq}) through the sensor;

$$I_{RD48} = (3.99 \times 10^{-17}\text{Acm}^{-1})\Phi_{eq}V, \tag{3.3}$$

yields the leakage current I_{RD48} measured at -10°C for a silicon-diode sensor, at its depletion voltage, of volume V and subjected to neutron fluence of Φ_{eq} [9]. The T-506 dosage of 6.17×10^{13} cm^{-2}, by Eq. (3.3), would cause a 300 micron thick sensor to develop a 73.8μAcm^{-2} leakage current. This differs from the experimentally obtained leakage current, 74.5μAcm^{-2}, by only 1%.

The agreement between experimental results and studies on neutron-induced damage with FLUKA simulations suggests that the damage to the T-506 sensor is predominantly neutron based rather than electromagnetic. Furthermore, this suggests that damage to the BeamCal will also be neutron dominated.

3.3 T-506 NIEL Deposition Density

Equivalent 1MeV fluence, although useful, is a clunky metric. It obfuscates the true source of damage in the sensor by presenting the damage as a 'damage-equivalence.' Assumption (1), the NIEL Scaling Hypothesis, states that damage to a sensor is directly proportional to the energy deposition in the detector and not particle fluence. I therefore quantize damage in terms of the total non-ionizing energy deposition density in the sensor. For a FLUKA output, this can be calculated by summing over each bin and evaluating the product of the respective NIEL and fluence,

$$\lambda_\rho \equiv \sum_{\text{bins}} \frac{\Phi(E,\theta)}{dEd\Omega}\text{NIEL}(E)dEd\Omega. \tag{3.4}$$

in units of MeV-g^{-1}, where $NIEL(E)$ is the NIEL function of Fig. 3.3. I then normalize this by the sensor material's density ρ (2.33 g/cm^3 for silicon), and define an "energy deposition density" λ:

$$\lambda \equiv \rho\lambda_\rho = \rho \sum_{\text{bins}} \frac{\Phi(E,\theta)}{dEd\Omega} \text{NIEL}(E) dEd\Omega \tag{3.5}$$

in units MeV-cm^{-3}.

In this way, I calculate the energy deposition density to be 8.37×10^{-4}MeV cm^{-3} per primary beam particle in the T-506 sensor. Since the T-506 delivered charge was $51\mu C$, or 3.25×10^{14} beam particles, the total energy deposition density was $\lambda_{T506} \equiv 2.66\times10^{11}$ MeV cm^{-3}. By assumption (3), leakage current is linearly proportional to dosage. Therefore a sensor subject to a volume energy deposition density λ will experience an area leakage current density linearly proportional to the T-506 dosage:

$$I(\lambda) = \frac{\lambda}{\lambda_{T506}} I_{T506}.$$

For example, for a silicon diode sensor operated at temperature T and close to depletion,

$$I(\lambda, T) = \frac{\lambda}{\lambda_{T506}} \sigma(T), \tag{3.6}$$

in units of A-cm^{-2} and making use of the fit $\sigma(T)$ for current density from Fig. 3.1. Below, estimates of λ from FLUKA simulations will be made use of in this expression to estimate the leakage current density draw as a function of exposure and operating temperature for the BeamCal instrument.

4

Results and Analysis - The BeamCal

I constructed the BeamCal within the FLUKA framework according to the ILC's detailed baseline design (see Fig. 4.1). A 3D rendering in SimpleGeo[1] is presented in Fig. 4.1. All of my simulations of the Beamcal model it as fifty layers of 0.25cm thick Tungsten radiators with 0.03cm thick Silicon detectors between each pair of Tungsten radiators. The Tungsten layers are separated by 0.07 cm face-to-face. Both Silicon and Tungsten layers are each cylindrical in shape with a radius of 15 cm. A 2.05cm radius hole is cut from the center of each layer and is called the 'exhaust pipe.' A 1.55cm radius hole, offset from the center by 4.57cm, is cut from each layer as well and is called the 'input pipe.' This is an approximation of the real design, where the input pipe is actually splayed at an angle of 14 mrad from the exhaust pipe, to allow for the small crossing angle electron-positron beam.

Simulations of the BeamCal use the same physics settings used for the T-506 simulation: PRECISIO defaults, use of the evaporation and photonuclear interaction models, and the biasing of photonuclear interactions.

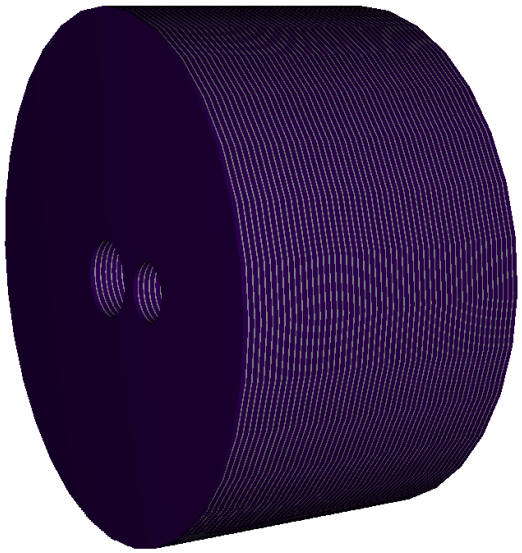

Figure 4.1: 3D rendering of the Beamline Calorimeter using SimpleGeo [1].

4.1 Comparisons to T-506

Although it is not necessary, it is interesting to compare the FLUKA neutron field between that of the T-506 experiment and the BeamCal. First, I compare the distribution of neutron energies in each FLUKA simulation as shown in Fig. 4.2. In the BeamCal simulation I used the entirety of Layer 12 as a scoring plane, and in the T-506 simulation the same scoring plane as from Section 3.1.

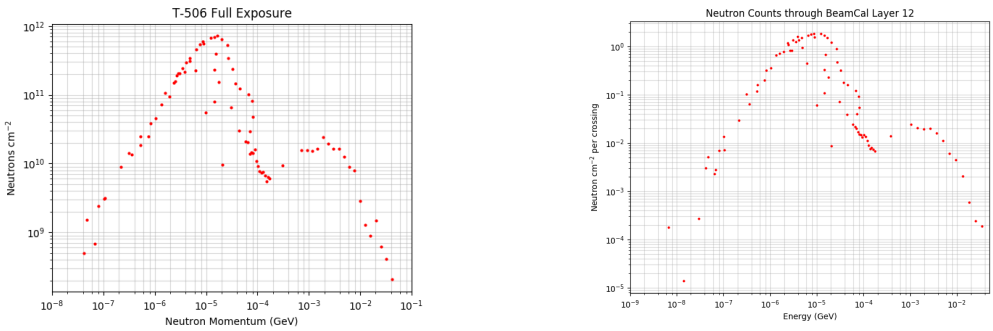

Figure 4.2: Comparison of fluences of neutrons vs energy for a full T-506 exposure (left) and a BeamCal bunch crossing (right).

Both neutron energy spectra peak at 10keV and 1 MeV and have similar forms. In fact, this reduces the reliance of BeamCal results on the energy dependence of the NIEL

scaling hypothesis.

Next, I investigate the contributions to fluence with respect to neutron angle-of-incidence, shown in Fig. 4.3. Although the neutron-production mechanism is isotropic, the volume that produces neutrons is not always so. In the T-506 apparatus, only the areas directly before and after the scoring plane receive an electromagnetic dosage and contribute to the neutron generation. The result is that the sensor only receives neutrons from angles $\theta \sim 0$ and π. In the BeamCal, the entire apparatus is exposed to the pair background, and so the majority of it contributes to the neutron field. An isotropic neutron field forms, and as a result the $\cos\theta$ denominator in Eq. (2.3) plays a large role: neutrons with angle of incidence $\theta \sim \frac{\pi}{2}, \frac{3\pi}{2}$ contribute more significantly. The energy deposition density metric accounts for this by quantizing damage with respect to total neutron path length. Note that this significantly increases the expected neutron NIEL in the BeamCal, and their associated damage effects relative to estimates based on naively scaling damage rates observed in the T-506 experiment.

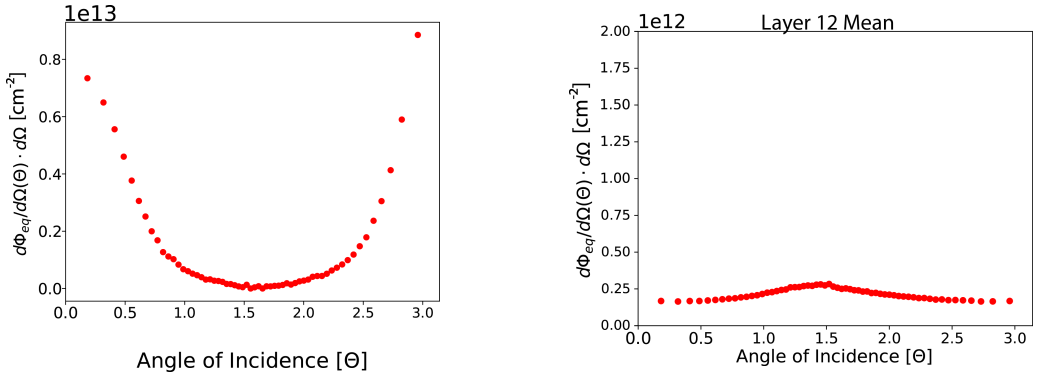

Figure 4.3: Comparison of fluences of neutrons vs angle (rad) for a full T-506 exposure (left) and a BeamCal bunch crossing (right).

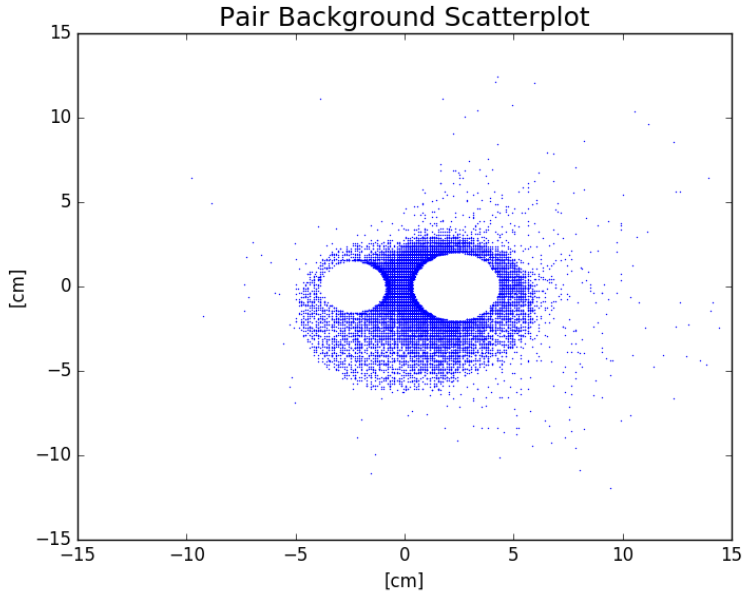

Figure 4.4: Pair background scatter plot on the forward face fo the BeamCal. Constituent particles of the background are plotted as dots.

4.2 Developed Neutron Field in BeamCal

The incident pair background is not homogeneous on the forward face of the BeamCal, as can be seen in Fig. 4.4. This non-homogeneity would imply that the neutron field would also be non-homogeneous, and understanding the position-dependence of damage to the BeamCal's sensors is important. Using the FLUKA `SCORE` card `USRBIN`, I scored neutron fluence in spacial bins for layers 2-13. The fluences are presented as heatmaps in Figures 4.5 through 4.7, where each colored pixel is a spacial bin.

`USRBIN` does not use angular effects in calculating particle fluence, however. Since we have seen that high angle of incidence neutrons contribute more significantly, `USRBIN` may not accurately portray the areas exposed ot the greatest neutron NIEL energy deposition.

It does, however, suggest which parts of which layers may be exposed to the highest fluence and neutron NIEL energy deposition. Since layer 12 seemed to have the highest fluence, I placed several small ($0.2 \times 0.2\text{cm}^2$) scoring planes across it. I also placed several

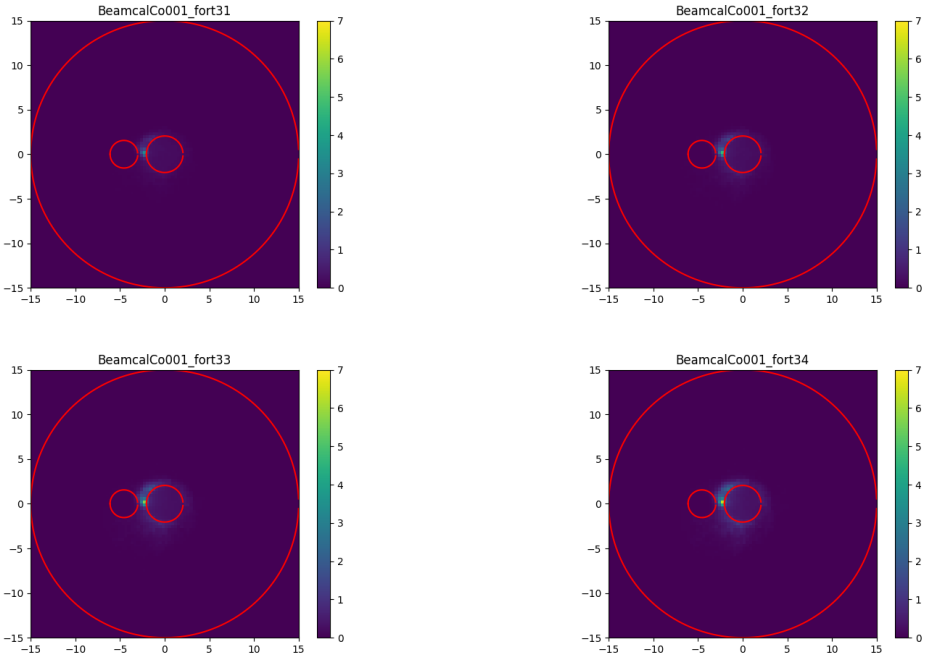

Figure 4.5: relative neutron fluence heat maps. Layer number starting from the top left going clockwise: 2, 3, 4, 5.

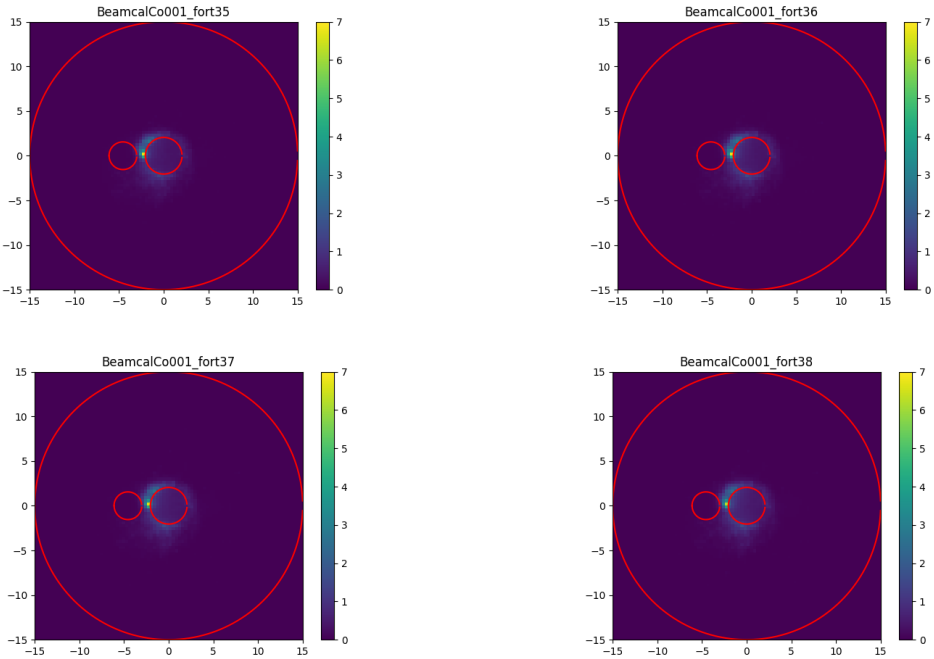

Figure 4.6: relative neutron fluence heat maps. Layer number starting from the top left going clockwise: 6, 7, 8, 9.

across layer 30 to compare how the neutron field changes with depth. See Fig. 4.8 for the arrangement of scoring planes. Neutrons were scored through these planes in the normal

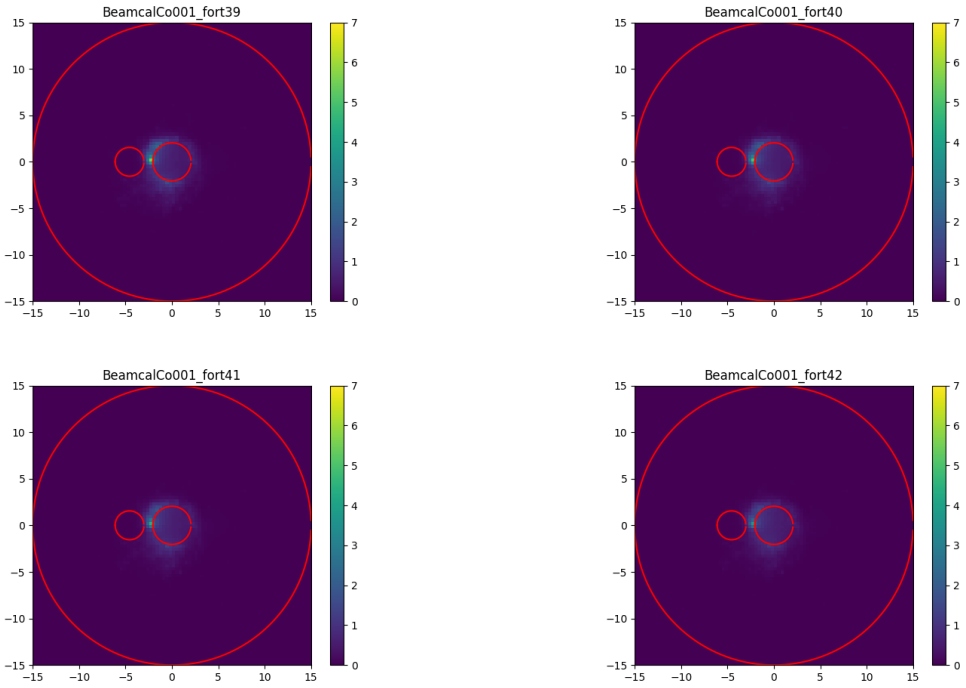

Figure 4.7: relative neutron fluence heat maps. Layer number starting from the top left going clockwise: 10, 11, 12, 13.

way using `USRBDX`. The relative neutron NIEL energy deposition density, compared to T-506, at each of these points is shown in Fig. 4.9.

From Figures 4.5 through 4.7, the most damaged regions appear would appear to be the the wedge-region between the input and exhaust pipes, and the region opposite to the exhaust pipe. Although the heat maps suggest the wedge region has a much greater particle count, Fig. 4.9 shows that instead the neutron NIEL falls off much more slowly as you move away from the wedge region. To illustrate why, 1MeV equivalent neutron fluence is graphed as a function of angle in the wedge region, the region opposite the exhaust pipe, and the region opposite the input pipe in Fig. 4.10. Thus the overall current and power draw in the BeamCal is larger and more spread out than one might naively suspect.

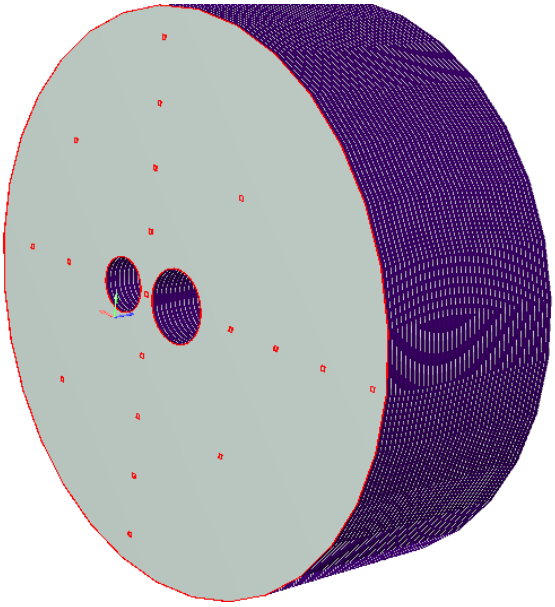

Figure 4.8: locatoins of the small scoring planes in Layers 12 and 30. Used to find spacial dependence of relative energy deposition density.

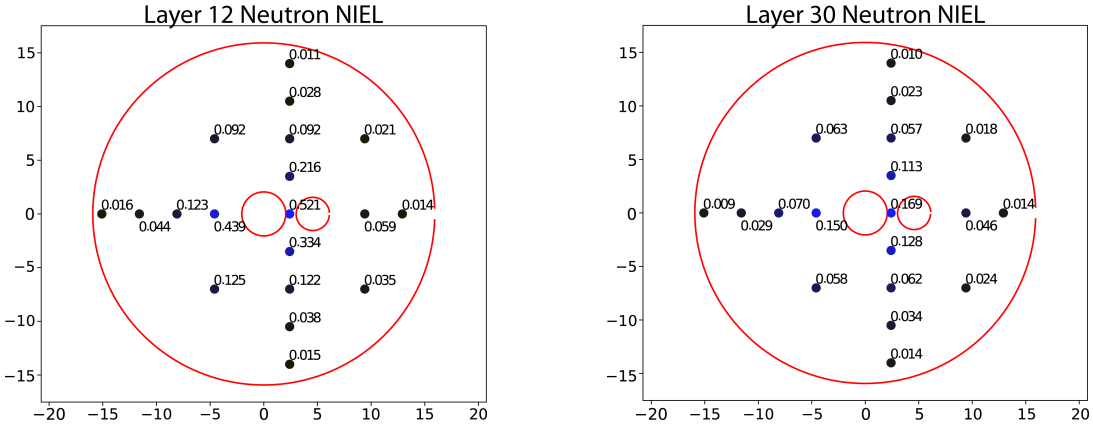

Figure 4.9: Relative energy deposition densities at various scoring planes in silicon sensor Layers 12 (left) and 30 (right) in the BeamCal. Numbers are calculated by finding energy deposition over a snow-mass year in the case of the BeamCal and dividing it by energy deposited in the T-506 experiment.

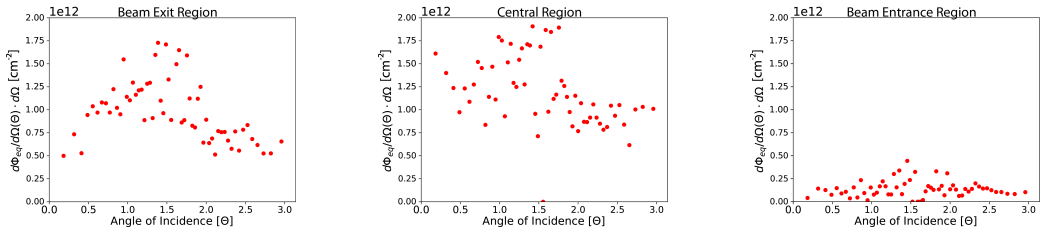

Figure 4.10: Neutron NIEL energy deposition with respect to neutron angle of incidence on silicon diode sensor layer 12 in three regions of the BeamCal. Left, opposite exhaust pipe; center, wedge region; right, opposite input pipe.

4.3 BeamCal Power Draw

Since power draw is directly dependent on leakage current ($P = IV$), predicting the total power draw requires calculating neutron energy deposition and then leakage current for each pixel in every layer in the BeamCal. Total power draw can then be calculated by summing individual leakage currents, and taking the product of this with the sensors' bias voltage.

This can be simplified, however, since the energy deposition for an entire layer can be expressed as the sum of the energy deposition of each pixel in the layer: $\Lambda = \lambda_1 + \lambda_2 + \ldots \lambda_n$. Each pixel is also equal area, and the sum of their areas is the area of the layer $A = a_1 + a_2 + \ldots + a_n = a \times n$.

Suppose $I(\lambda_i)$ is the leakage current through a pixel after λ_i MeV are deposited per cubic centimeter. For some layer,

$$I_{tot} = A \sum_{i=1}^{n} I(\lambda_i).$$

And since current draw is linear with respect to λ

$$I_{tot} = AI\left(\sum_{i=1}^{n} \lambda_i\right) = AI(\Lambda), \tag{4.1}$$

and so the total leakage current for a layer can be calculated from the total energy deposited on that layer.

By introducing single scoring planes comprising the entire surface of each of the BeamCal layers, FLUKA can be configured to score the mean fluence through entire detector layers for a given duration of ILC operation. This can be turned into an average neutron-induced NIEL energy deposition density λ, and by Eq. (3.6) a layer-average leakage

current. That is,

$$I_L(\lambda, T) = \frac{\lambda}{\lambda_{T506}} A\sigma(T)$$

in units of amps, where A is the area of a layer, $\sigma(T)$ is the current density measured for the T-506 WSI-P4 sensor (see Fig. 3.1), and $\lambda_{T506} = 2.7 \times 10^{11}$ MeV-cm^{-3} is the neutron-induced NIEL dose endured by the T-506 WSI-P4 sensor. We assume the thickness of the BeamCal sensor is the same as that of the WSI-P4 sensor, 300 μm.

Calculating power draw is straight forward given the leakage current and bias voltage (600V), and the results are presented in Fig. 4.11 for several temperatures. By summing the wattage over all layers, I found that the total power draw of the entire BeamCal will be 82 Watts after one year of operation, with wattages for other temperatures presented in Table 4.1.

Temperature [°C]	Power Draw [Watts]
-7.5	105
-10	82
-15	50
-20	30

Table 4.1: Power draw accumulation of the BeamCal at various temperatures per Snowmass year of operation, or 10^7 seconds.

4.4 Radially Mounted Electronics

To study the effects of the BeamCal on the electronics surrounding it, I placed eight scoring planes radially around the BeamCal. They were arranged such that the scoring planes are normal to the axis of the BeamCal, and four were placed around each the twelfth and thirtieth Tungsten radiators in angular increments of $\pi/2$ radians.

I scored charged pions, electrons, positrons, protons, neutrons and anti-protons through

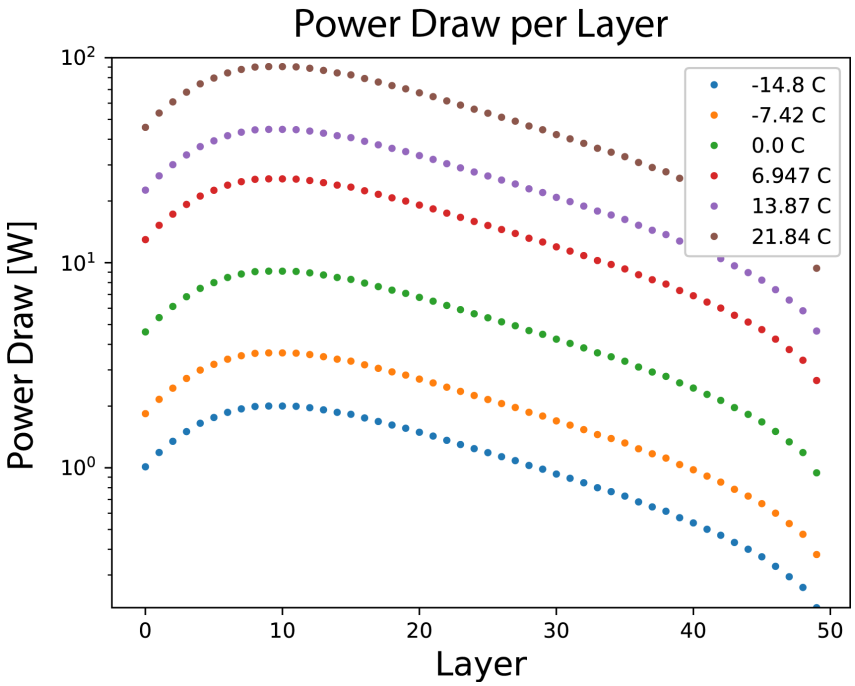

Figure 4.11: Power draw in the BeamCal after operating for one Snowmass year, showing a range of operating temperatures. One Snowmass year represents a number of primaries in 10^7 seconds of ILC operation.

each of these scoring planes over the pair backgrounds from two bunch crossings. Fig. 4.12 shows the neutron and electron/positron fluences scaled for one Snowmass year of operation. The radial scoring planes counted zero protons, anti-protons, or charged pions; suggesting an upper bound on each of these fluences of 10^{10} per Snowmass year. This same upper bound also applies to electrons and positrons around layer 30.

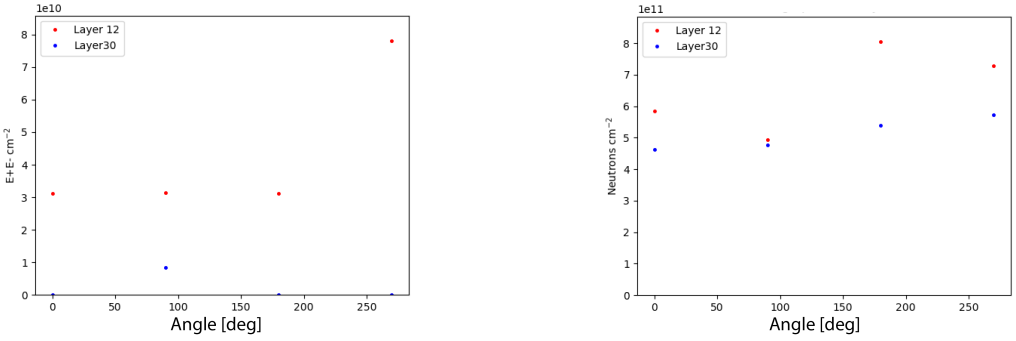

Figure 4.12: Fluences (electron/positron left, neutron right) over one Snowmass year through scoring patches around the BeamCal. Zero degrees corresponds to the direction opposite the input pipe.

5

Conclusions

5.1 Summary

Making use of FLUKA simulations to extrapolate experimental results from T-506 we have estimated the accumulated power draw of the ILC BeamCal as a function of operating temperature and exposure. At an operating temperature of -10°C we estimate a power draw accumulation of about 100 Watts per year of operation. Making use of the energy dependence observed in T-506, we expect that this power draw accumulation could be reduced to around 15 Watts per year if the BeamCal is operated at -30 °C, the proposed operating temperature for the inner silicon layers of the upgraded Atlas detector at the Large Hadron Collider.

We also estimated the fluence of particles in the region outside the BeamCal. The total dose was well below that expected to cause concern for the electronics.

5.2 Future Work

5.2.1 Neutron Backscattering

The BeamCal has been shown to be a neutron source. Although these neutrons may not be significantly damaging to the BeamCal, it may prove a threat to the ensemble of trackers and calorimeters, seen in Fig. 1.2, upstream of the BeamCal. This project, called the 'neutron backscattering problem,' proved to be beyond the scope of this paper.

In short, using the same BeamCal model and a modified `MGDRAW` user routine, one can prepare a list of neutrons exiting the front of the BeamCal due to the pair background of a single bunch crossing. This list is called 'collision tape.'

One could then use the DESY `lcio.py` script[1] to convert the collision tape into a form readable by the LCIO GEANT4 simulation framework. There, it should be possible to study the effects of the BeamCal on a detector in which the BeamCal is nested.

5.2.2 Neutron Absorption

If the neutron backscattering problem proves too damaging, it may be useful to line the front of the BeamCal using a low-Z[2] layer of neutron-absorbing material. Boron-10 seems to be an ideal candidate material.

FLUKA and my BeamCal model would prove useful to study how well such a lining can attenuate the neutron flux out of the BeamCal. One should also verify that FLUKA can accurately calculate the neutron-absorption cross-section of arbitrary materials.

[1] available online

[2] a high-Z material would make another neutron source

Bibliography

[1] Theis, C. and Buchegger, K.H. and Brugger, M. and Forkel-Wirth, D. and Roesler, S. and Vinke, H. Interactive three dimensional visualization and creation of geometries for Monte Carlo calculations, 2006.

[2] George Courcoubetis et al. Updated Results of a Solid-State Sensor Irradiation Study for ILC Extreme Forward Calorimetry. In *Proceedings, International Workshop on Future Linear Colliders (LCWS15): Whistler, B.C., Canada, November 02-06, 2015*, 2016.

[3] A Ferrari, Paola R Sala, A Fassò, and Johannes Ranft. *FLUKA: A multi-particle transport code (program version 2005)*. CERN Yellow Reports: Monographs. CERN, Geneva, 2005.

[4] T.T. Böhlen, F Cerutti, M.P.W Chin, A Fassò, A Ferrari, P.G Ortega, A Mairani, P.R Sla, G Smirnov, and V Vlachoudis. *The FLUKA Code: Developments and Challenges for High Energy and Medical Applications*. `CERN-2005-10 (2005), INFN/TC_05/11, SLAC-R-773`

[5] D. Schulte. Beam-beam simulations with GUINEA-PIG. 1999.

[6] V Vlachoudis. *FLAIR: A Powerful But User Friendly Graphical Interface For*

FLUKA. Proc. Int. Conf. on Mathematics, Computational Methods & Reactor Physics (M&C 2009). CERN, Saratoga Springs, New York, 2009.

[7] The International Commission on Radiation Units and Measurements. *Journal of the International Commission on Radiation Units and Measurements*, 11(1):NP, 2011.

[8] A. Vasilescu (INPE Bucharest) and G. Lindstroem (University of Hamburg). Displacement damage in silicon, on-line compilation, 2006.

[9] G Lindström et al. Radiation hard silicon detectors - developments by the rd48 (rose) collaboration. *Nuclear Instruments and Methods in Physics Research Section A: Accelerators, Spectrometers, Detectors and Associated Equipment*, 466(2):308 – 326, 2001. 4th Int. Symp. on Development and Application of Semiconductor Tracking Detectors.